Journal of Materiomics 6 (2020) 643–650

Contents lists available at ScienceDirect

Journal of Materiomics

journal homepage: www.journals.elsevier.com/journal-of-materiomics/

Opinion paper

Bio-inspired flexible vibration visualization sensor based on piezo-electrochromic effect

Xuan Chen [a], Laihui Luo [b], Zhou Zeng [c], Jie Jiao [c], Mudassar Shehzad [a], Guoliang Yuan [a], Haosu Luo [c], Yaojin Wang [a, *]

[a] School of Materials Science and Engineering, Nanjing University of Science and Technology, Nanjing, 210094, Jiangsu, China
[b] Department of Microelectronic Science and Engineering, Ningbo University, Ningbo, 315211, China
[c] Shanghai Institute of Ceramics, Chinese Academy of Sciences, 215 Chengbei Road, Jiading, Shanghai, 201800, China

ARTICLE INFO

Article history:
Received 9 March 2020
Received in revised form
27 April 2020
Accepted 5 June 2020
Available online 16 June 2020

Keywords:
Piezoelectric
Ferroelectric single crystals
Flexible electronics
Vibration sensor
Electrochromic

ABSTRACT

Monitoring structural vibration can provide quantitative information for both structural health evaluations and early-warning maintenance. The most classic vibration-based structural health monitoring is equipped with piezoelectric accelerometers, which is expensive and inconvenient due to cumbersome and time-consuming sensor installation and high power-consumptive data acquisition systems. One other main challenge with these systems is the inherent limitations for multi-point monitoring in critical elements with curvature due to their non-conformability. Here, inspired by the chameleon, we report a cost-effective, flexible and conformal, self-powered vibration sensor based on elasto-electro-chemical synergistic effect of piezoelectricity and electrochromism. The sensor can provide not only *in-situ* visualization, but also *ex-situ* recording of structural vibration due to the non-volatile color memory effect of electrochromism. The passive sensor system is composed of two distinct electronic components — ternary $Pb(In_{1/2}Nb_{1/2})O_3$–$Pb(Mg_{1/3}Nb_{2/3})O_3$–$PbTiO_3$ piezoelectric single crystal ribbon sensors and a solid-state tungsten trioxide electrochromic indicator driven by vibration-induced voltage generated by the piezoelectric ribbons. The proposed piezo-electrochromic based passive non-volatile visualization sensor may find diverse applications in structural health monitoring, smart wallpapers, and medical injury rehabilitation.

1. Introduction

Mechanical vibration is the principal source of damage in engineering structures, such as bridges, dams, aircraft, and wind-turbines. As such, considerable efforts have been devoted to vibration-based structural health monitoring (SHM) techniques [1–3], a powerful diagnostic tool for rapid condition-screening. The objective of SHM is to provide quantitative information pertaining to the integrity of the structure, especially components that are especially prone to damage or where such damage could lead to systemic failure [3]. Various techniques have been employed for structural health monitoring, including traditional techniques such as contact-type displacement or strain sensors, piezoelectric vibration sensors, fiber optic sensors, and more emergent techniques like noncontact-type vision-based cameras, drones, or robotic sensors [4].

Among the available SHM techniques, the piezoelectricity-based vibration sensors, equipped with data acquisition and conditioning electronics comprise the current state-of-the-art, with advantages including non-destructive sensing, high-sensitivity, and fatigue-free performance [3,5]. However, traditional piezoelectric-based systems are highly expensive and inconvenient to implement due to cumbersome and time-consuming sensor installation. Furthermore, system power requirements significantly increase the life-time cost for long-term *in-situ* monitoring applications. For some special applications where in-situ data processing is not feasible (e.g. tunnel, subsurface mine or underwater buildings) it would be beneficial if the structural health monitoring system provides a means for ex-situ vibration monitoring [6,7], such as through a color change [8,9]. A Javery and colleagues recently report a user-interactive electronic skin that can realize the instantaneous pressure visualization on a polyimide substrate, which is capable of

* Corresponding author.
E-mail address: yjwang@njust.edu.cn (Y. Wang).
Peer review under responsibility of The Chinese Ceramic Society.

https://doi.org/10.1016/j.jmat.2020.06.002

transducing the applied pressure into brightness, rather than processing traditional electric signals [10]. However, vibration-induced color change of this electronic skin sensor require a constant voltage bias, which in turn leads to a high power consumption [11,12]. Z.L. Wang and colleagues demonstrated a pressure visualization and recording system via the piezotronic effect of ZnO [13], in which the electrochromic device can be colored and bleached without the assistance of a computer. However, the piezoelectric effect of ZnO is notable weaker than the perovskite oxides, such as $Pb(Zr,Ti)O_3$ ceramics and $Pb(Mg_{1/3}Nb_{2/3})O_3$-$0.3PbTiO_3$ single crystals [14–16], and in turn the sensitivity and prospect of this complicated system to detect structural vibration is unknown.

Another obstacle of piezoelectric vibration sensors in structural health monitoring applications is a trade-off between their spatial resolution and cost, especially since the spatial coverage of such systems is determined by the number of installed piezoelectric vibration sensors. Additionally, because most of state-of-the-art high-sensitivity piezoelectric sensors are based on rigid and brittle perovskite oxides, such as $Pb(Zr,Ti)O_3$ ceramics, these sensors are non-conformal and severely limited in monitoring of critical curve-shaped elements [15] (Fig. S1). To address the non-conformability challenge of piezoelectric vibration sensors, several different approaches are feasible - including mechanical thinning to micro-meter scales [17,18], the use of flexible organic piezoelectric materials [19], one-dimensional nanowires [20–24], and flexible thin films [25–29]. The mechanical polishing approach is considered to be the most effective and convenient. Since the micro-sized flexible piezoelectric ribbons have the same composition and microstructure as their respective bulk versions, the thinned versions retain the extraordinary piezoelectric performances of their bulk counterparts [29]. In particular, it has been reported that self-powered biomedical devices were achieved assisted by high-performance mechanical-to-electrical energy harvest via mechanical polishing approach [17,30].

The current limitations in traditional piezoelectric-based materials and systems complicate the realization of practical and cost-effective structural heath monitoring systems that can be applied on critical curved elements and to provide *ex-situ* recording of structural vibration. Here, we introduce a device inspired by the chameleon that incorporates a synergy effect between piezoelectricity and electrochromism that can provide *in-situ* vibration sensing, while also recording the degree of vibration as a visible color change in an element of the sensor. The piezo-electrochromic color changing structural health monitoring sensor is demonstrated in a flexible, attachable heterostructure, and is realized without external power consumption.

Some animals can change their skin color in response to external stimulus, which helps them to hide themselves and to evade enemies, increasing chances for survival [33]. The chameleon, for example (Fig. 1a) can change the color of skin pigment cells by changing the size of epidermal cells in response to external stimuli [34]. Inspired by this unique stimuli-responsive color-changing ability of the chameleon, we developed a vibration visualization sensor that transforms environmental mechanical energy into electrical signals, and subsequently to a color change through the synergy of piezoelectric and electrochromic effects. Fig. 1b illustrates the proposed flexible vibration visualization sensors composed of a high-efficiency, flexible piezoelectric generator (PEG), a rectifier, and a flexible electrochromic device (ECD). The PEG is fabricated based on $Pb(In_{1/2}Nb_{1/2})O_3$–$Pb(Mg_{1/3}Nb_{2/3})O_3$–$PbTiO_3$ (PIN-PMN-PT) single crystal ribbons that are bonded with two flexible circuits on an acrylonitrile-butadiene-styrene (ABS) substrate. As shown in Fig. 1c, the change of mechanical stress causes polarization reorientation in the piezoelectric component and in turn converts mechanical energy into alternating electric energy, and the rectifier turns the alternating electric voltage to direct electric voltage. The structure of flexible multi-layered ECD is illustrated Fig. 1d, which comprised of WO_3 film, gel electrolyte ITO and PET. Under a negative bias, the injection of electrons and small cations into the WO_3 film from the electrolyte. The rectifier circuit converts the alternating electric voltage to direct electric voltage, enabling a cumulative color change in the electrochromic indicator. The proposed synergistic effect of piezoelectricity and electrochromism is an alternative multi-field coupling of elasto-electro-chemistry [35] —the piezo-induced voltage autonomously drives the chemical potential in electrochromic indicator, which provides an extra functionality of *in-situ* sensing and *ex-situ* recording the incident structural vibration.

2. Experimental

2.1. Fabrication of PIN-PMN-PT piezoelectric generator

We cut a (110)-oriented single crystalline PIN-PMN-PT into a block that was bonded to a glass substrate with wax melted at 60 °C. The PIN-PMN-PT block was thinned to 45 μm by grinding and chemical-mechanical polishing [36]. Top and bottom (Au) electrodes were deposited after each polishing process. The sheets were diced into $[001]^L \times [1\text{–}10]^W \times [110]^t$ PIN-PMN-PT cuboid plates with a size of 20 × 2 × 0.045 mm shown as Fig. S2. The sample was heated to the melt temperature of the adhesive wax to take the PIN-PMN-PT plates off the glass substrate. A poling process was performed in the PIN-PMN-PT plates along their thickness directions under electric field of 10 kV/cm in a silicon oil bath. Then two flexible circuits and ten cuboid plates were placed together to form a sandwich-structure and bonded using high-strength epoxy into array. Finally the integrated array was stick on an ABS flexible substrate to completely fabricate the flexible piezoelectric generator (Fig. S3a).

2.2. Preparation of WO_3

The WO_3 film was prepared on a transparent ITO-coated PET substrate by using DC magnetron sputtering under the fabrication condition of 12.5:25 O_2:Ar, 1.8 Pa pressure, 100 W power and 40 min sputtering time. The sputtering target was tungsten with the purity 99.95%, whose diameter and thickness are 60 mm and the 3 mm respectively.

2.3. Preparation of the gel polyelectrolyte

We weighed $LiClO_4$, acetonitrile (ACN), poly (methyl methacrylate) (PMMA) in the weight proportion of 3:50:10 respectively. Subsequently, $LiClO_4$ was completely dissolved in acetonitrile and PMMA mixed slowly into the solution at the same time. The temperature and time of stirring are respectively 65 °C and 10 h until the electrolyte became gel state.

2.4. Assembly of WO_3 electrochromic device

The gel polymer electrolyte was dropped on the prepared WO_3 film/ITO/PET that performed as working electrode. A piece of ITO/PET film was placed on top as the counter-electrode and assembled together. Then the ECD was dried naturally in air for 2 h to form a sandwich-type device [32].

2.5. Structure and properties characterization

The phase structure of WO_3 film was characterized by X-ray diffraction (XRD, Bruker D8), and the micro-area analysis was

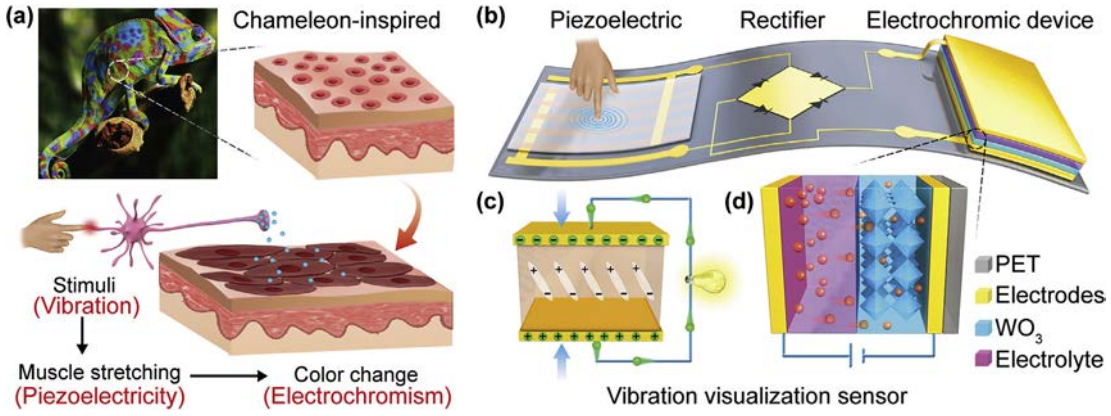

Fig. 1. Schematic illustration of bio-inspired piezo-electrochromic effect concept and the sensor design framework. (a) The biological principal of chameleon camouflage in response to mechanical stimuli and parallel in the piezo-electrochromic regime. (b) Illustration of the flexible passive vibration-visualization sensor framework, which comprises a piezoelectric generator, an electrochromic indicator, and a voltage rectifier. The proposed bio-inspired piezo-electrochromic effect is a synergy between (c) piezoelectricity (i.e., induction of electrical signals under mechanical stimuli) [31] and (d) electrochromism (i.e, color change by cation-injection) [32]. The chameleon image is from https://pangeanimales.com/.

carried out using a transmission electron microscope (TEM, Titan G2 60–300). The cross-sectional quality and the surface morphology were respectively obtained by scanning electron microscopy (SEM, ZEISS Merlin) and an atomic force microscope (AFM, Bruker Multimode 8) respectively. X-ray photoelectron spectroscopy (XPS, Thermo ESCALAB 250XI) was used for elemental analysis. The Raman spectra in pristine and colored states was recorded using a Raman spectroscope (Aramis). The electrochromic performances and transmittance spectra of WO_3 film were measured using an electrochemical workstation (CIMPS, Zahner) and a UV–vis spectrophotometer (UV-3600) respectively. The piezoelectric performance test system is shown in Fig. S3b. A linear shaker, driven by an amplified function generator output was used to drive the PIN-PMN-PT piezoelectric sensor. The open-circuit voltage was measured via a Tektronix Digital Oscilloscope (TBS1104), a charge amplifier (Kistler Type5018) and a precision impedance analyzer (Agilent 4294), while the short-circuit current was directly measured using a source meter (Keithley 2635).

3. Results and discussion

The piezoelectric characterization of the PIN-PMN-PT piezoelectric generator is performed through periodic bending/unbending motions using a custom-designed shaker. The integrated measurement system used to characterize its electromechanical energy conversion performances is shown in Fig. S3. The output of the electric signals have been measured as functions of vibration frequency, amplitude, and waveform shape. Fig. 2a shows the linear increment of piezoelectric voltage with the strain at 4 Hz sinusoidal bending. The open-circuit voltage increases from 8 V to 30 V as the strain increases from 0.068% to 0.302%, where the strain was determined by the thickness of device and step displacement of shaker under the assumption of radius bending [29,37], as shown in Fig. S3b. It can be found that the increase of open-circuit voltage is slightly smaller than the proportional values of the strain increase, which might be because partial stress was released in the middle of the device (i.e., the gap between the heads of two PIN-PMN-PT), especially at large strain conditions. At constant strain, the open-circuit voltage also increases from 10 V to 30 V along with the frequency from 1 Hz to 5 Hz (Fig. S4a), which agree well with previous piezoelectric generator [37]. A high short-circuit current of 110 μA was obtained in response to 0.302% bending deformation at 4 Hz (Fig. 2b), which was recorded using Keithly 2635A source meter. The sensor response to impulse oscillation is almost consistent with sine wave bending mode (Figs. S4b and c) in terms of output voltage and current. For a vibration visualization sensor, the change in color of ECD is directly related to the output energy of the PEG. The instantaneous current (I) signal is measured as a function of the external loading resistance (R) (Fig. 2c). The output current gradually decreases from 92 μA to 0.02 μA as R increases from 100 Ω to 1 GΩ. The calculated voltage (U) increases from 9.2 mV to 20 V over the same range. As a result, the instantaneous power can be calculated through the formula $P = I^2R$, which varies as a function of the external loading resistances, as shown in Fig. 2d. The power increases first and then decreases with the increase of the loading resistance, reaching a maximum value of 610 μW at $R = 165$ kΩ, while the current and voltage are 61 μA and 10 V, respectively. Based on the maximum power transfer theorem [17,26,29], it can be concluded that the external loading resistance of $R = 165$ kΩ is matched with impedance of piezoelectric energy harvesting, where the output power reach maximum.

To characterize the electric power generation, a capacitor of 1 μF was charged through periodic bending and unbending of PEG with the assistance of a rectifier circuit (Fig. S5a). The measurement is schematically demonstrated in Fig. S5b. Fig. 2e shows the real-time voltages of the capacitor which is charged by PEG at 4 Hz under different bending strains. The data show a rapid rise in voltage during the initial stage of charging process and a gradual approach to a saturation value. The voltage of the capacitor reaches saturation in almost 30 s under the cyclic bending of the high output performance PEG. The increase in bending strain from 0.068% to 0.302% at 4 Hz results in a significant increase in saturation voltage from 9 V to 27 V. The real-time voltage curves of a 10 μF) charged at different frequencies and of different capacitor values charged under the identical conditions are given in Figs. S5c and d, respectively. The correlation of saturation voltage with frequency is in accordance with the result of Fig. 2e, which indicates that the capacitor can be charged more rapidly from with increasing bending strain or higher frequency.

Fig. 3 shows the microstructure characterization of the WO_3 film prepared by DC magnetron sputtering. X-ray diffraction (XRD) was applied to examine the phase structure of the WO_3 film. As shown in Fig. 3a, the diffraction peak of WO_3 film coincides with those of ITO/PET substrates, and no additional diffraction peaks of WO_3 were observed. The X-ray diffraction profile of the pure WO_3 film (inset of Fig. 3a), which was deposited on glass substrates under the

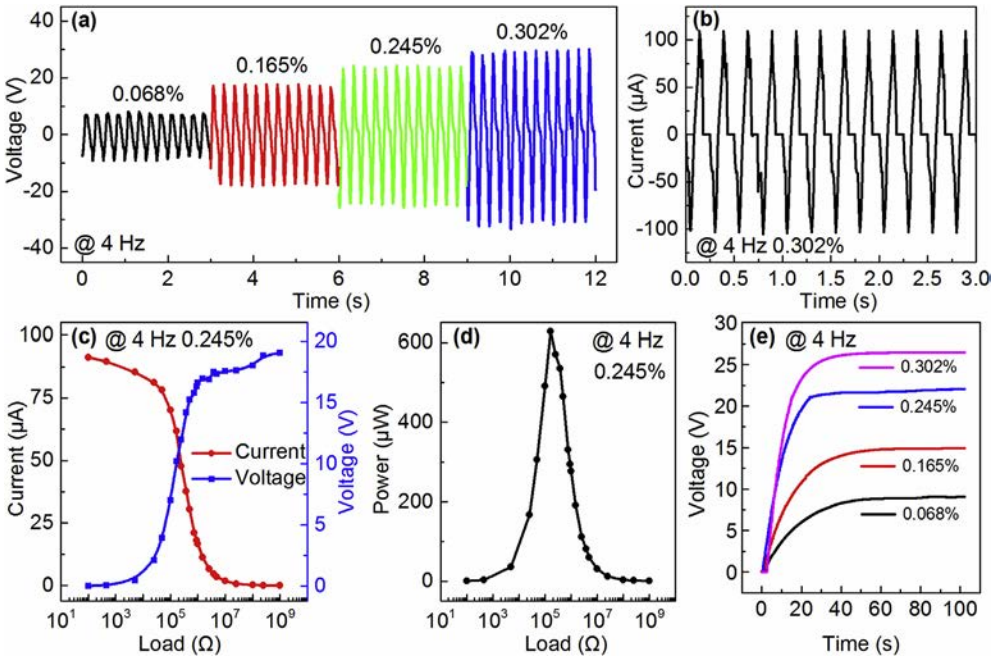

Fig. 2. The properties of the flexible PIN-PMN-PT piezoelectric generator. (a) The open-circuit voltages at different bending strains at 4 Hz under sine wave. (b) The short-circuit current generated from the PEG. (c) The measured output currents and corresponding voltage under different resistances of external load. (d) The relationship between the calculated instantaneous power and loading resistances. (e) The real-time voltages of the capacitor while charged at different bending strains.

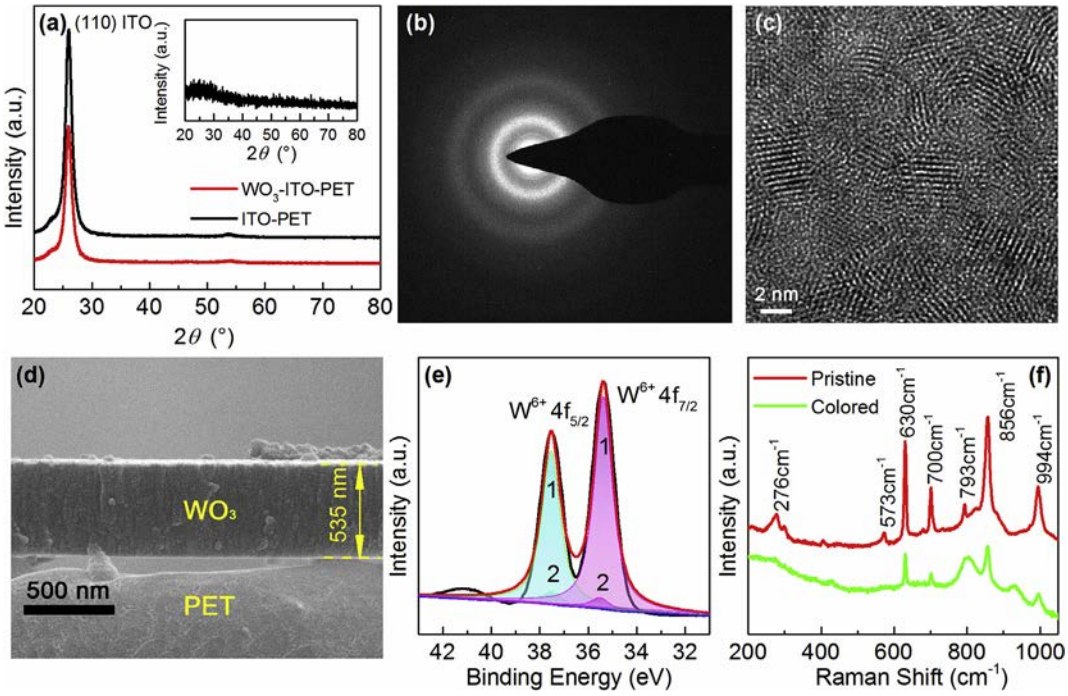

Fig. 3. The microstructure characterization of the WO_3 film. (a) The XRD pattern of WO_3 film on ITO/PET substrates and a contrastive diffraction pattern of ITO/PET (the inset shows the XRD pattern of WO_3 film on glass substrates). (b) The selected area electron diffraction (SAED) pattern of the WO_3 film. (c) A TEM image of WO_3 film. The scale bar is 2 nm. (d) The cross-sectional SEM graph of WO_3 film. (e) The XPS spectra of W element. (h) The Raman spectra of the WO_3 film in pristine and colored states.

same condition, shows a broad peak without any diffraction peaks around WO_3 [38]. A halo ring is represented in the selected area electron diffraction (SAED) pattern (Fig. 3b), which is in agreement with the results of the XRD pattern. As shown in Fig. 3c, the high-resolution TEM image clearly shows that the tungsten oxide WO_3 film is in nanocrystalline structure, in which nanocrystalline regions with several nanometer size are randomly distributed (red-circle designated in Fig. S6a). It has been previously reported that amorphous WO_3 films have a higher coloration efficiency and faster color/bleach time than its crystalline structure [39], While the localized nanocrystalline distribution of WO_3 improves the stability for electrochromic applications in some degree [40]. Fig. 3d shows

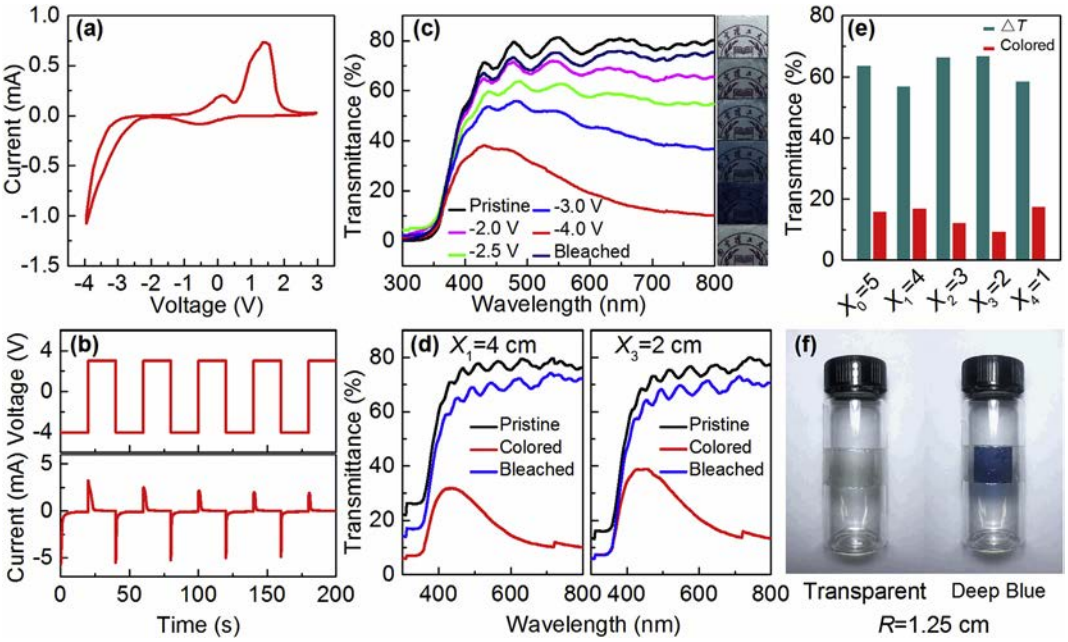

Fig. 4. Properties of the all-solid flexible WO_3 ECD. (a) Cyclic voltammogram of the WO_3 ECD with a $LiClO_4$/ACN/PMMA gel electrolyte, cycled between −4.0 and 3.0 V at a scan rate of 100 mV/s. (b) Chronoamperometry curves of the WO_3 ECD measured at −4 V/+3 V for 20 s. (c) Transmittance spectra and optical images of the WO_3 ECD in colored and bleached states under potentials of −4.0 V, −3.0 V, −2.5 V, −2.0 V, 0 V and +3.0 V. (d) Transmittance spectra of the WO_3 ECD in two different curved states, applied potential from −4 V to +3 V. (e) Transmittance change and transmittance after −4 V colored of the WO_3 ECD under flat and different curved states at 633 nm. (f) Photograph of the WO_3 ECD adhered to a curved surface with a radius of 1.25 cm.

the cross-sectional SEM graph of WO_3 film with thickness of ~535 nm. The heterostructure of PET/ITO/WO_3 and their interface is obviously seen based on the SEM image via focused ion beam (Fig. S6 b, c).

The binding energy and valence states in the WO_3 film were studied by X-ray photoelectron spectroscopy (XPS). The two spin–orbit split peaks of W $4f_{7/2}$ and W $4f_{5/2}$ in black lines can be observed at ~37.7 and 35.5 eV (Fig. 3e), respectively. The two main peaks at 37.5 and 35.4 eV are associated with W^{6+} oxidation states and the weaker peaks originate from the W^{5+} component [41].

Fig. 3f shows the Raman spectroscopy for WO_3 film in pristine and colored states, which is used to determine the inner chemical bonds change of WO_3 before and after the injection of electrons and small cations. The peaks at the wavenumber region of 600–900 cm^{-1} are attributed to the vibrations of O–W^{6+}–O modes, while those around 573 cm^{-1} and 994 cm^{-1} in the pristine state arise from peroxo groups in (WO_2). The intensity of peaks at 630 cm^{-1},700 cm^{-1},793 cm^{-1} and 856 cm^{-1} decrease after coloration because of W ion reduction from +6 to +5 [42]. Simultaneously, the peaks in low wavenumber regions increase, which are assigned to the W^{5+} or W^{4+} oxygen bonds. The change of the Raman spectroscopy reflects valence state variation of W ion in the electrochromic process. These microstructure analyses indicate that the WO_3 films prepared on the flexible ITO/PET substrate by DC magnetron sputtering possess excellent quality.

To realize the vibration visualization sensor, tungsten oxide (WO_3) was used as the functional layer of ECD due to its good coloration efficiency, high response, and stability. The redox reaction occurs due to injection and extraction of electrons and cations into WO_3 films under electrical potential which eventually changes the color of ECD. The redox reaction of WO_3 in a Li^+ electrolyte can be represented through the following reversible chemical equation. Li^+ cations and electrons are injected into the WO_3 film by applying a negative voltage to the ITO/PET substrate. As a result, WO_3 is reduced to Li_xWO_3, changing it's the substance from transparent to the blue [43,44]. At a positive bias, the Li^+ cations and electrons are extracted from Li_xWO_3, reversibly bleaching the film to the transparent state.

$$WO_3 + xe^- + xLi^+ \leftrightarrow Li_xWO_3$$

Cyclic voltammograms of the WO_3 film in 1 mol/L $LiClO_4$ propylene carbonate solution were recorded under different scan rates of 25, 50 and 100 mV/s as shown in Fig. S7a. Under applied voltage from 0 V to −2 V, the initial transparent WO_3 film gradually turns blue, and then it is reversibly bleached and returns to transparent state as the voltage increases up to +2 V. In Fig. S7b, cyclic voltammogram after bending 2000 and 5000 times shows little change from the original curve, indicating that the WO_3/ITO/PET film has good mechanical fatigue behavior. The corresponding transmittance spectra of WO_3 film were recorded at 0 V, −1 V, −2 V and +2 V, as shown in Fig. S7c. At a wavelength of 633 nm, the initial transmittance is 80% and the transmittance is restored to 70% after the film bleached under forward bias. The transmittance is 30% at −1 V and 5% at −2 V coloration indicating modulation up to 75%. The transmittance of colored WO_3 films at different times after removing the applied voltage is shown in Fig. S7d. It is worth noting that the variation in transmittance of WO_3 film is around or less 0.5% even after 1 h. The blue color of the WO_3 film can be maintained around one day since the transmittance at the wavelength of 633 nm was still 28% after 600 min, termed as "color-memory effect" [13], indicating the WO_3 film has the capacity to record the application of electric voltage, and potential for vibration visualization sensor under the piezoelectricity induced electric voltage.

To prepare an all-solid flexible electrochromic devices, we replaced the liquid electrolyte with a polyelectrolyte. A classic gel-type ACN-$LiClO_4$-PMMA electrolyte was used due to its easy processing, good mechanical strength, wide range of working

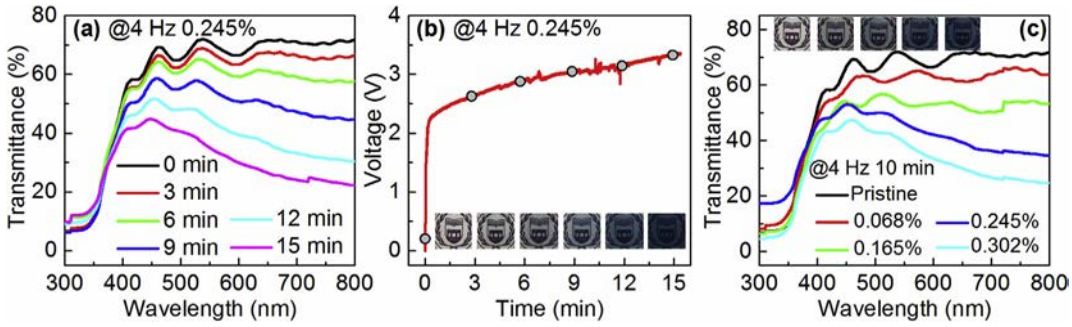

Fig. 5. The performance of flexible vibration visualization sensor. (a) Transmittance spectra of the vibration visualization sensor obtained at various vibration durations. (b) The real-time voltage of the ECD while colored by PIN-PMN-PT piezoelectric generator. Insets are the corresponding color contrast pictures at different time points. (c) Transmittance spectra and corresponding optical images of the vibration visualization sensor obtained at different bending strains.

temperatures, and enhanced stability [45]. The ECD was fabricated by assembling a WO_3 film with two ITO electrodes and a gel electrolyte in a sandwich structure [32]. Fig. 4a shows the cyclic voltammogram of the ECD in the potential range of −4 V to +3 V with a scan rate of 100 mV/s. As the ion migration rate drops in the gel electrolyte, the colored and bleached voltages increase and the current reduces in the cyclic voltammogram. The current response of ECD from −4 V to +3 V for 20 s is represented in Fig. 4b. The switching time of ECD is defined as the time that is required to reach up to 90% of its full response [46]. According to chronoamperometry curves in Fig. 4b, we recorded the coloration time (t_c) and the bleaching time (t_b) as 2.35 s and 3.75 s respectively. The fast switching speed is competitive to most all-solid electrochromic devices due to its large interface between the WO_3 film and electrolyte [47], which also enable the proposed sensor to provide *in-situ* vibration visualization.

The transmittance spectra of the WO_3 ECD was measured under several different applied voltages in the wavelength range of 300 nm–800 nm. The transmittance change indicates that the appearance of the ECD transforms from transparent (bleaching) to deep blue (coloration), as shown on the right photographs of Fig. 4c. Under a negative potential, the WO_3 film turns to blue and the color darkens as the potential becomes more negative. The transmittance modulation −4 V is 64% at 633 nm, which can be easily observed with the naked eye. On reversing the voltage, the ECD returns to the transparent state with a decline of only 4.6% of its transmittance at 633 nm at 3 V (compared with the pristine). Fig. 4d shows the transmittance modulation of tungsten oxide based ECD in two different curved states. The overall length of ECD in a flat condition is 5 cm. When the end-to-end distance under bending (as illustrated in Fig. S8) is either 4 cm or 2 cm, there is negligible change in the shape and position of the transmittance modulation curves, indicating good flexibility of the ECD. The color contrast and transmittance of ECD at 633 nm wavelength at −4 V under flat and different curved states is summarized in Fig. 4e. The transmittance modulation is recorded as 64%, 57%, 66%, 67% and 59% with decrease of the end-to-end distance X, respectively, which suggests that the change in color is almost independent of the degree of curvature [32]. It is worth noting that the curvature independent color change indicates the sensor can be applied in different curvature structure. As shown in Fig. 4f, the image of fabricated ECD adhered to a transparent glass bottle of radius 1.25 cm displays the clear color contrast from transparent to blue. Furthermore, these results indicate the excellent electrochromic performance of flexible tungsten oxide ECD even under its bending state [32].

To realize the vibration visualization, we integrate the flexible PIN-PMN-PT piezoelectric generator (PEG) and WO_3 electrochromic device (ECD) with a rectifier to monitor and record ambient vibrational energy. Fig. 5a depicts the transmittance spectra measured on the interval of every 3 min by applying a bending vibration of 4 Hz and 0.245% on PEG. The corresponding real-time voltage and color contrast photographs of ECD are also presented in Fig. 5b and the gray dots on curve corresponds six time points in Fig. 5a. The voltage of ECD increases from 0 V to 3.5 V under continuous ambient vibration conditions for 15 min. The transmittance modulation reaches 40% at 633 nm with increasing potential on the ECD, inducing a vibration-induced color contrast from transparent to deep blue that is distinguishable by the naked eye. Furthermore, we will be able to monitor the vibration history because of the color memory effect of WO_3 shown as Fig. S7d. We also measured the spectroscopic change of the ECD when applying different bending strains from 0.068% to 0.302%. Each time the pressure on the vibration visualization sensor was sustained for 10 min and the transmittance spectra was subsequently recorded. The transmittance at 633 nm decreased with increasing pressure, resulting in a gradual deepening in color (inset of Fig. 5c). Therefore, color darkening of the initially transparent vibration visualization sensor indicates the intensity of vibration, and may serve as a visual warning. Please note that the sensor cannot distinguish the harmful vibration amplitude and frequency low than couple of Hz, because both can produce an identical voltage to drive the electrochromic indicator (Figs. 2e and S5c). However, the significance of the proposed sensor is to provide visual information for the historical vibration with both harmful amplitude and frequency. These results demonstrate the feasibility of transforming ambient vibration to visible color change by flexible vibration visualization sensor integrating piezoelectric generator (PEG) and electrochromic device (ECD).

4. Conclusions

In conclusion, a self-powered vibration visualization sensor based on a synergy between the piezoelectric effect and electrochromism is realized in a flexible system by integrating a ternary PIN-PMN-PT piezoelectric single crystal ribbon and a solid-state Tungsten trioxide electrochromic indicator. The piezoelectric generator exhibits an open-circuit voltage of above 20 V, a short-circuit current of 92 μA and a maximum electric output power of 610 μW under an excitation bending strain of 0.245% at frequency of 4 Hz. The solid-state WO_3 electrochromic film device exhibited fast switching speed with coloration time of 2.35 s and bleaching time of 3.75 s, good flexibility with curvature-independent coloration and blenching contrast, and good mechanical fatigue properties. The flexible/attachable system demonstrated that the

external vibration can be directly sensed and visualized by color changes of the WO_3 films due to the non-volatile color memory effect of electrochromism. In turn, the proposed self-powered piezo-electrochromic-based vibration visualization sensor may have cost-effective and convenient applications in structural health monitoring, smart wallpapers, and medical injury rehabilitation without cumbersome, time-consuming installation and high power-consuming data acquisition systems, especially for early-warning maintenance of critical curvature structures suffering from harmful vibration.

Declaration of competing interest

The authors declare that they have no known competing financial interests or personal relationships that could have appeared to influence the work reported in this paper.

Acknowledgements

This work was supported by the National Natural Science Foundation of China (11874032, 51790492 and 51911530120), the Fundamental Research Funds for the Central Universities (30918012201), and the Opening Project of Key Laboratory of Inorganic function material and device, Chinese Academy of Sciences (KLIFMD-201801).

Appendix A. Supplementary data

Supplementary data to this article can be found online at https://doi.org/10.1016/j.jmat.2020.06.002.

References

[1] Feng DM, Feng MQ. Experimental validation of cost-effective vision-based structural health monitoring. Mech Syst Signal Process 2017;88:199–211.
[2] Magalhaes F, Cunha A, Caetano E. Vibration based structural health monitoring of an arch bridge: from automated oma to damage detection. Mech Syst Signal Process 2012;28:212–28.
[3] Carden EP, Fanning P. Vibration based condition monitoring: a review. Struct Health Monit 2004;3(4):355–77.
[4] Sony S, Laventure S, Sadhu A. A literature review of next-generation smart sensing technology in structural health monitoring. Struct Contr Health Monit 2019;26(3):e2321.
[5] Koruza J, Bell AJ, Frömling T, Webber KG, Wang K, Rödel J. Requirements for the transfer of lead-free piezoceramics into application. J Materiomics 2018;4:13–26.
[6] Zhang Y, Fang Y, Li J, Zhou Q, Xiao Y, Zhang K, et al. Dual-mode electronic skin with integrated tactile sensing and visualized injury warning. ACS Appl Mater Interfaces 2017;9(42):37493–500.
[7] Wang D, Chen X, Yuan G, Jia Y, Wang Y, Mumtaz A, et al. Toward artificial intelligent self-cooling electronic skins: large electrocaloric effect in all-inorganic flexible thin films at room temperature. J Materiomics 2019;5(1):66–72.
[8] Sun J, Pu X, Jiang C, Du C, Liu M, Zhang Y, et al. Self-powered electrochromic devices with tunable infrared intensity. Sci Bull 2018;63(12):795–801.
[9] Yang X, Zhu G, Wang S, Zhang R, Lin L, Wu W, et al. A self-powered electrochromic device driven by a nanogenerator. Energy Environ Sci 2012;5(11):9462–6.
[10] Wang C, Hwang D, Yu Z, Takei K, Park J, Chen T, et al. User-interactive electronic skin for instantaneous pressure visualization. Nat Mater 2013;12(10):899–904.
[11] Chou H-H, Nguyen A, Chortos A, et al. A chameleon-inspired stretchable electronic skin with interactive colour changing controlled by tactile sensing. Nat Commun 2015;6(1):1–10.
[12] He Z, Gao B, Li T, Liao J, Liu B, Liu X, et al. Piezoelectric-driven self-powered patterned electrochromic supercapacitor for human motion energy harvesting. ACS Sustainable Chem Eng 2018;7(1):1745–52.
[13] Han X, Du W, Chen M, Wang X, Zhang X, Li X, et al. Visualization recording and storage of pressure distribution through a smart matrix based on the piezotronic effect. Adv Mater 2017;29(26):1701253.
[14] Li F, Cabral MJ, Xu B, Cheng Z, Dickey EC, LeBeau JM, et al. Giant piezoelectricity of Sm-doped $Pb(Mg_{1/3}Nb_{2/3})O_3$-$PbTiO_3$ single crystals. Science 2019;364(6437):264–8.
[15] Wang Y, Luo C, Wang S, Chen C, Yuan G, Luo H, et al. Large piezoelectricity in ternary lead-free single crystals. Adv Electro Mater 2020;6:1900949.
[16] Yang N, Chen X, Wang Y. Magnetoelectric heterostructure and device application. Acta Phys Sin 2018;67(15):232–47.
[17] Geon-Tae H, Hyewon P, Jeong-Ho L, SeKwon O, Kwi-Il P, Myunghwan B, et al. Self-powered cardiac pacemaker enabled by flexible single crystalline PMN-PT piezoelectric energy harvester. Adv Mater 2014;26(28):4880–7.
[18] Chen Y, Zhang Y, Zhang L, Ding F, Schmidt OG. Scalable single crystalline PMN-PT nanobelts sculpted from bulk for energy harvesting. Nanomater Energy 2017;31:239–46.
[19] Lee J-H, Lee KY, Kumar B, Nguyen Thanh T, Lee N-E, Kim S-W. Highly sensitive stretchable transparent piezoelectric nanogenerators. Energy Environ Sci 2013;6(1):169–75.
[20] Lee YB, Han JK, Noothongkaew S, Kim SK, Song W, Myung S, et al. Toward arbitrary-direction energy harvesting through flexible piezoelectric nanogenerators using perovskite $PbTiO_3$ nanotube arrays. Adv Mater 2016;29(6):1604500.
[21] Sun H, Zhang Y, Zhang J, Sun X, Peng H. Energy harvesting and storage in 1D devices. Nat Rev Mater 2017;2(6):1–12.
[22] Qin Y, Wang X, Wang ZL. Microfibre-nanowire hybrid structure for energy scavenging. Nature 2008;451(7180):809–13.
[23] Lee S, Hong JI, Xu C, Lee M, Kim D, Lin L, et al. Toward robust nanogenerators using aluminum substrate. Adv Mater 2012;24(32):4398–402.
[24] Cheng LQ, Li JF. A review on one dimensional perovskite nanocrystals for piezoelectric applications. J Materiomics 2016;2(2):25–36.
[25] Yeo HG, Ma X, Rahn C, Trolier-McKinstry S. Efficient piezoelectric energy harvesters utilizing (001) textured bimorph PZT films on flexible metal foils. Adv Funct Mater 2016;26(32):5940–6.
[26] Wang D, Yuan G, Hao G, Wang Y. All-inorganic flexible piezoelectric energy harvester enabled by two-dimensional mica. Nanomater Energy 2018;43:351–8.
[27] Yu X, Wang H, Ning X, Sun R, Albadawi H, Salomao M, et al. Needle-shaped ultrathin piezoelectric microsystem for guided tissue targeting via mechanical sensing. Nature Biomedical Engineering 2018;2(3):165–72.
[28] Gao W, Zhu Y, Wang Y, et al. A review of flexible perovskite oxide ferroelectric films and their application. J Materiomics 2019;6:1–16.
[29] Park KI, Son JH, Hwang GT, Jeong CK, Ryu J, Koo M, et al. Highly-efficient, flexible piezoelectric PZT thin film nanogenerator on plastic substrates. Adv Mater 2014;26(16):2514–20.
[30] Hwang G-T, Kim Y, Lee J-H, Oh S, Jeong CK, Park DY, et al. Self-powered deep brain stimulation via a flexible PIMNT energy harvester. Energy Environ Sci 2015;8(9):2677–84.
[31] Wang Y, Wen X, Jia Y, et al. Piezo-catalysis for nondestructive tooth whitening. Nat Commun 2020;11(1):1–11.
[32] Park H, Kim DS, Hong SY, Kim C, Yun JY, Oh SY, et al. A skin-integrated transparent and stretchable strain sensor with interactive color-changing electrochromic displays. Nanoscale 2017;9(22):7631–40.
[33] Zhao Q, Wang Y, Cui H, Du X. Bio-inspired sensing and actuating materials. J Mater Chem C 2019;7(22):6493–511.
[34] Isapour G, Lattuada M. Bioinspired stimuli-responsive color-changing systems. Adv Mater 2018;30(19):1707069.
[35] Kalinin SV, Spaldin NA. Functional ion defects in transition metal oxides. Science 2013;341(6148):858–9.
[36] Hwang G-T, Yang J, Yang SH, Lee H-Y, Lee M, Park DY, et al. A reconfigurable rectified flexible energy harvester via solid-state single crystal grown PMN-PZT. Adv Energy Mater 2015;5(10):1500051.
[37] Zeng Z, Xia R, Gai L, Wang X, Lin D, Luo H, et al. High performance of macro-flexible piezoelectric energy harvester using a $0.3PIN\text{-}0.4Pb(Mg_{1/3}Nb_{2/3})O_3\text{-}0.3PbTiO_3$flake array. Smart Mater Struct 2016;25(12):125015.
[38] Madhavi V, Kondaiah P, Hussain OM, Uthanna S. Structural, optical and electrochromic properties of RF magnetron sputtered WO_3 thin films. Phys B Condens Matter 2014;454:141–7.
[39] Zheng H, Ou JZ, Strano MS, Kaner RB, Mitchell A, Kalantar-zadeh K. Nanostructured tungsten oxide - properties, synthesis, and applications. Adv Funct Mater 2011;21(12):2175–96.
[40] Lee SH, Deshpande R, Parilla PA, Jones KM, To B, Mahan AH, et al. Crystalline WO_3 nanoparticles for highly improved electrochromic applications. Adv Mater 2006;18(6):763–6.
[41] Cong S, Tian Y, Li Q, Zhao Z, Geng F. Single-crystalline tungsten oxide quantum dots for fast pseudocapacitor and electrochromic applications. Adv Mater 2014;26(25):4260–7.
[42] Santato C, Odziemkowski M, Ulmann M, Augustynski J. Crystallographically oriented mesoporous WO_3 films: synthesis, characterization, and applications. J Am Chem Soc 2001;123(43):10639–49.
[43] Zhang B, Hou C, Wang H, et al. Preparation and performance of reduced graphene oxide functionalized flexible and multicolor electrothermal chromatic films. J Inorg Mater 2018;33(11):1232–6.
[44] Liu N, Liu S, Geng F. Two-dimensional tungstate nanosheets for constructing novel photochromic hydrogel with ultrahigh flexibility. J Materiomics 2018;4(2):144–8.
[45] Ganesh GPT, Deb B. Designing an all-solid-state tungsten oxide based electrochromic switch with a superior cycling efficiency. Adv Mater Interfaces 2017;4(14):1700124.
[46] Wang S, Dou K, Zou Y, Dong Y, Li J, Ju D, et al. Assembling tungsten oxide hydrate nanocrystal colloids formed by laser ablation in liquid into fast-response electrochromic films. J Colloid Interface Sci 2017;489:85–91.
[47] Zhang J, Tu J-p, Xia X-h, Wang X-l, Gu C-d. Hydrothermally synthesized WO_3

nanowire arrays with highly improved electrochromic performance. J Mater Chem 2011;21(14):5492–8.

Xuan Chen received her B.S. degree from Nanjing University of Science and Technology in 2017. She is currently pursuing her M.S. degree in the School of Materials Science and Engineering, Nanjing University of Science and Technology, China, under the supervision of Prof. Yaojin Wang. Her research focuses on the flexible inorganic ferroelectric films and their applications on sensors.

Guo-Liang Yuan is currently a professor in the School of Materials Science and Engineering, Nanjing University of Science and Technology, China. He received his Ph.D degree from Nanjing University in 2004. Then he joined Department of Applied Physics, The Hong Kong Polytechnic University and worked as an Alexander von Homboldt research fellow in Bonn University from 2006 to 2007 and JSPS research fellow in Tsukuba University from 2008 to 2009. He joined Nanjing University of Science and Technology in 2009. His research focuses on ferroelectric, piezoelectric, and multiferroic thin films and devices.

Haosu Luo, professor, and the group leader of ferroelectric single crystals and devices at Shanghai Institute of Ceramics, Chinese Academy of Sciences. He has significantly contributed to the growth and development of piezoelectric single crystals, especial for the growth and practical application of PMN-PT single crystals in the world. Current researches involve the growth of high-Tc relaxor-based single crystals, lead free piezoelectric single crystals, and their device applications on ultrasonic transducers, infrared detectors, magnetoelectric magnetic sensors, and various device applications. He is a pioneer in the world for the single crystal growth of piezoelectric materials and devices fabrication. He has developed many innovative technologies for the growth and application of PMN-PT single crystals. He has involved more than 500 publications, and the H-impact index is 37 for his publications. He was nominee of EEE-UFFC Ferroelectrics Recognition Award in 2014 and 2015. He acquired the National Award for Technological Invention 2nd Prize in 2005, and the first prize of natural science of Shanghai municipal government in 2013.

Yaojin Wang is a Professor in the School of Materials Science and Engineering, Nanjing University of Science and Technology, deputy director of MIIT Key laboratory of Advanced Display Materials and Devices. He is severing as Associate Editor of Journal of American Ceramic Society. He received his Ph.D. degree in Shanghai Institute of Ceramics, Chinese Academy of Science in 2010. He was jointly educated in Hongkong Polytechnic University from Mar. 2007 to Sept. 2008 and worked in Virginia Tech as a Postdoc Research Associate from Aug. 2010 to Aug. 2015. His research focuses on: Integrated magnetoelectric heterostructures for applications of magnetic sensors and bioelectronics; flexible ferro-electronics and devices; process, properties and physics of ruggedized ferroelectric materials. He has authored or coauthored over 100 peer-reviewed papers.